Dependence of Creep Strength on Cooling Rate After Subsolvus Solution Treatment in Wrought Alloy 718

Satoru Kobayashi, Chuuya Aoki, Tomonori Ueno and Masao Takeyama

Abstract It was recently found that the creep strength and creep life of wrought alloy 718 samples showed an interesting dependence on the cooling rate in the standard subsolvus solution temperature: the time to 0.2% creep strain varies from 5 to 400 h depending on the cooling rate between 1 and 199 °C/min with the maximum value at an intermediate cooling rate of 51 °C/min under a creep condition of 621 °C/724 MPa. In the present paper, microstructures were observed for samples after creep deformation to 0.2% creep strain to understand the dependence of the creep strength on the cooling rate. The microstructural observations using *a* field emission type scanning electron microscope and transmission electron microscope showed that the size of coherent γ''/γ' precipitates in grains decreased and the number density increased with increasing the cooling rate but they saturated around the cooling rate at which the creep strength was maximized. A careful observation on grain boundaries revealed that the precipitation of fine γ'' phase precipitates was enhanced along grain boundaries and coherent twin boundaries at intermediate cooling rates and that of δ phase platelets was pronounced along grain boundaries and incoherent twin boundaries at slower cooling rates. These microstructural features suggest that the maximized creep strength is related to an enhanced precipitation of γ''/γ' particles along grain/twin boundaries as well as a high number density (fine size) of fine γ''/γ' particles in grain interiors.

Keywords Microstructure · Grain boundaries · γ''/δ-Ni_3Nb phase

S. Kobayashi (✉) · M. Takeyama
Tokyo Institute of Technology, Tokyo, Japan
e-mail: kobayashi.s@mtl.titech.ac.jp

C. Aoki · T. Ueno
Hitachi Metals Ltd, Osaka, Japan

© The Minerals, Metals & Materials Society 2018

E. Ott et al. (Eds.), *Proceedings of the 9th International Symposium on Superalloy 718 & Derivatives: Energy, Aerospace, and Industrial Applications*, The Minerals, Metals & Materials Series, https://doi.org/10.1007/978-3-319-89480-5_28

Introduction

Alloy 718 is *the* most widely used Ni based wrought superalloy for high temperature components such as aircraft engine and land-base gas turbine disks because of good mechanical properties and fabricability etc. [1, 2]. The microstructure of this alloy contains several types of second phase*s* of δ-Ni_3Nb ($D0_a$), γ″-Ni_3Nb ($D0_{22}$) and γ′-$Ni_3(Al,Ti)$ ($L1_2$) etc. in the γ-Ni (A1) solid solution matrix, which is controlled to obtain the mechanical properties that are required for particular high temperature components.

The standard heat treatment adopted for this alloy, *the* so-called subsolvus heat treatment, is a solution treatment below the δ solvus temperature above which the δ-Ni_3Nb ($D0_{22}$) phase is completely dissolved, followed by rapid cooling, and a subsequent two-step aging heat treatment (holding at 718 °C for 8 h, furnace cooling to 621 °C and holding at the temperature for a total aging time of 18 h followed by air cooling) [3, 4]. This subsolvus solution treatment is intended to form fine recrystallized grains pinned by residual δ phase precipitates in order to obtain good fatigue resistance. *Rapid* cooling from the solution treatment temperature is speculated to cause the precipitation of fine γ″/γ′ phase in the matrix phase not during the cooling but in the two-step aging heat treatment in order to obtain high strength. Creep properties might have been of secondary importance for the conventional use of the *alloy* treated with the subsolvus heat treatment, but the relative importance of creep properties to fatigue properties should increase in near future due to an increased temperature in turbine disks to meet a requirement to improve the efficiency of aircraft engines.

Aoki et al. recently found that a wrought alloy 718 sample showed an interesting dependency of creep properties on the cooling rate after the subsolvus solution treatment temperature; the time to 0.2% creep strain and the creep life showed a maximum value at an intermediate cooling rate under a creep condition of 621°C/724 MPa. The lower creep strength at slower cooling rates allows us to expect that the dependence is related to the precipitation of coherent γ″/γ′ particles within grains, but the lower creep strength at higher cooling rates *raises* a question on what microstructural factor causes the strength. In the present paper, microstructures were observed for samples after creep deformation to a creep strain of 0.2% to understand the dependency of the creep strength on the cooling rate.

Experimental Procedures

The alloy used was a hot-forged and ring-rolled 718 alloy. The chemical composition, analyzed by ICP-OES, is shown in Table 1. The rolled sample was cut by electro discharged machining into cylindrical specimens of 14 mm in diameter and 150 mm in length along the circumferential direction of the rolled sample parallel to

Table 1 Chemical compositions of the alloy 718 specimen [5]

Chemical compositions/wt%									
C	Ni	Cr	Mo	Co	Al	Ti	Nb	B	Fe
0.022	54.07	18.09	2.97	0.27	0.52	0.99	5.4	0.004	Bal.

the length of the cylinders. The specimens were solution treated at a temperature of 982 °C for 1 h, and cooled at different cooling rates between 1 and 199 °C/min to 600 °C *by gas quenching*, followed by air cooling. *The cooling rates were selected to investigate the effect of cooling rate that can be applicable to real forging parts. The measurements of cooling rates were made with a thermocouple inserted to a hole in a dummy sample with the same size. Each cooling rate shown is the averaged one between 982 and 600 °C.* The solution treated specimens were subsequently aged in the two-step standard condition (holding at 718 °C for 8 h, furnace cooling to 621 °C and holding at the temperature for a total aging time of 18 h followed by air cooling).

Creep tests were conducted at a temperature of 621°C under a constant load to have an initial stress of 724 MPa in air to a creep strain of 0.2% and to rupture. Samples were taken for microstructural observations from the gauge portion of the creep-interrupted specimens. The observation was performed using *a* field emission type scanning electron microscope (FESEM) and transmission electron microscope (TEM). The sample surface was prepared for FESEM observation by mechanical grinding and polishing down 1 μm sized diamond suspension, followed by electro-polishing with 10% perchloric acid in acetic acid. The sample for TEM observation was prepared by a twin-jet method using a solution of 10% perchloric acid in methanol.

Results and Discussion

Creep Properties

The creep strength and the creep life greatly vary as a function of the cooling rate from the solution treatment temperature, as shown in Fig. 1. The time to 0.2% creep strain varied from 5 to 400 h depending on the cooling rate between 1 and 199 °C/min with a maximum value at an intermediate cooling rate of 50 °C/min under the creep condition. The creep rupture time also shows a similar dependence on the cooling rate to the short time creep strength behavior with a maximum rupture time at somewhat shorter cooling rate. Table 2 summarizes the time to reach 0.2% creep strain and to rupture of the 718 alloy specimens obtained in the present study.

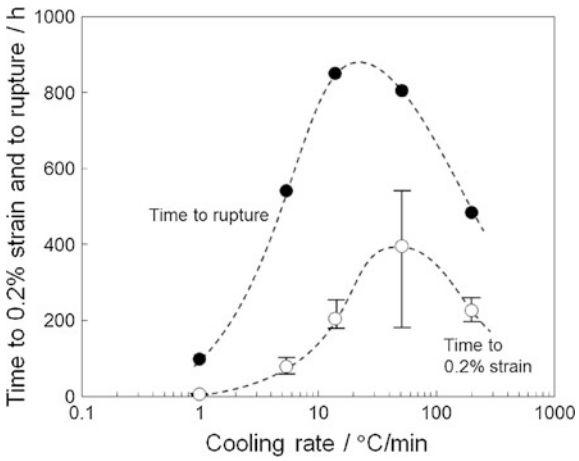

Fig. 1 Creep curves of the aged alloy 718 specimens with different cooling rates from solution treatment

Table 2 Creep properties of the alloy 718 samples cooled at different cooling rates from solution treatment and subsequently aged

Cooling rate (°C/min)	Time to 0.2% strain (h)[a]	Time to rupture (h)[b]
199	225.2	483
51	395.9	804.7
14	204.6	849.5
5.4	78.9	540.8
1	5.3	96.7

[a]The average value of the three tests
[b]N = 1

Microstructural Characterization

FESEM and TEM observations revealed that the microstructures along grain boundaries as well as in grains in the specimens depend on the cooling rate from the subsolvus solution treatment, especially in the morphology and distribution of δ and γ″ phase precipitates.

Figure 2 shows grain structures and distribution of δ phase precipitates in some of the creep-interrupted specimens at a low magnification of backscattered electron (BSE) imaging. It is seen that the matrix grain sizes are almost equivalent and their average size was ~14 μm regardless of the cooling rate. δ phase precipitates, imaged in bright contrast, are elongated and are 10 μm at maximum in size along their longitudinal directions, and their size and volume fraction increase slightly with decreasing the cooling rate. The size of δ phase precipitates and their dependence on the cooling rate allow us to deduce that the precipitates exist at the solution temperature and grew during cooling according to the cooling rate.

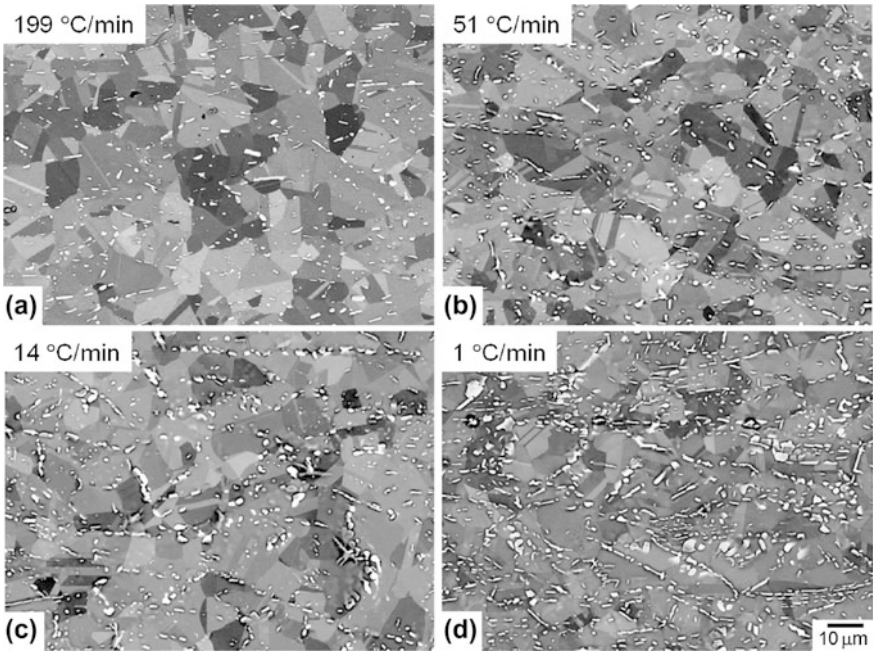

Fig. 2 Backscattered electron images taken from the gauge portion of the alloy 718 samples after 0.2% creep strain: **a** 199 °C/min, **b** 51 °C/min, **c** 14 °C/min, **d** 1 °C/min

Figure 3 shows the existence of precipitates at grain boundaries of the specimens at a high magnification of BSE imaging. Fine acicular precipitates as well as coarse ones are recognized at grain boundaries in the specimens of relatively slow cooling rates (Fig. 3c, d), *while only fine precipitates are seen at grain boundaries in the specimens of relatively fast cooling rates (Fig. 3a, b). These morphological features and the heat treatment profiles indicate that the fine/acicular precipitates are δ phase ones that were formed during cooling from the solution treatment temperature*. Figure 4 shows the distribution of precipitates in the matrix grains and at grain/twin boundaries *on* a high magnification secondary electron *image* on strongly etched sections. Fine grain-like precipitates are seen not only in grain interiors but also at grain boundaries and coherent twin boundaries, and the precipitation at the boundaries becomes more pronounced as the cooling rate decreases. The fine grain-like precipitates are presumed to be γ'/γ'' phase, according to their morphology based on a common knowledge in microstructure formation in alloy 718. Acicular precipitates, identified as δ phase, are also recognized at non-coherent twin boundaries that are twin boundaries, which divide twin-oriented grains but do not coincide with any crystallographic (111) planes, in the specimens of slow cooling rates.

TEM observations also revealed a dependence of the distribution of grain-boundary precipitates on the cooling rate. Figure 5 shows examples of TEM

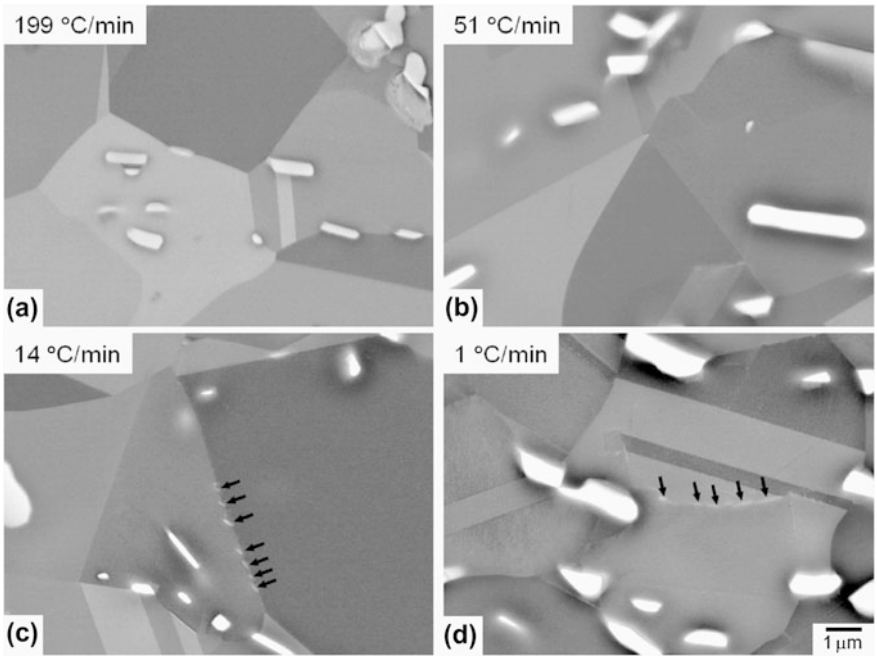

Fig. 3 Backscattered electron images taken from the gauge portion of the alloy 718 samples after 0.2% creep strain: **a** 199 °C/min, **b** 51 °C/min, **c** 14 °C/min, **d** 1 °C/min

micrographs including high angle grain boundaries. Misorientaion at grain boundaries was identified with selected are diffraction patterns (SADPs) obtained from *neighboring* grains, examples of which are shown in Fig. 5c. Our observation found no significant enhancement in precipitate density at grain boundaries in the specimen with the highest cooling rate of 199 °C/min (Fig. 5a, b), but *found* a concentration of precipitates along grain boundaries in the specimen with the cooling rate of 51 °C/min (Fig. 5c, d). Precipitates of a few hundred μm in size were observed on grain boundaries in the specimens with a slower cooling rate of 1 °C/min, as shown in Fig. 5e, f. The precipitates observed at grain boundaries are identified as γ″ phase and δ phase in the specimen of 51 °C/min and 1 °C/min, respectively, based on their morphologies.

Microstructural observations *of* grain interiors using TEM revealed that the size of coherent γ″/γ′ particles decreased and the number density increased with increasing cooling rate but *the size* saturated around the cooling rate at which the creep strength shows a maximum. Figure 6 shows typical TEM images together with SADPs. Fine needlelike (platelike) precipitates of 20–30 nm in size are formed such that they are orthogonally arranged in the specimens with *the higher* cooling rates of 199 and 51 °C/min. *These* precipitates were identified as γ″ phase with the $D0_{22}$ structure that *were* coherently formed with a crystallographic orientation relationship of $\{001\}_{\gamma}//(001)_{\gamma''}$ on the three (111) planes in the γ matrix phase as

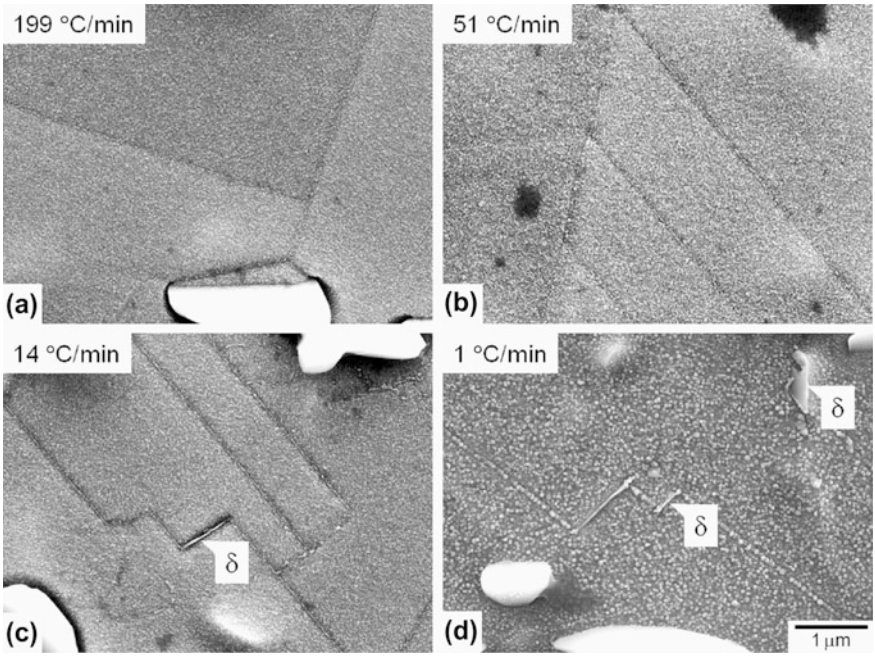

Fig. 4 Secondary electron images taken from the gauge portion of the alloy 718 samples after 0.2% creep strain: **a** 199 °C/min, **b** 51 °C/min, **c** 14 °C/min, **d** 1 °C/min. The section was strongly etched

habit plane, according to our crystallographic analysis on the SADPs obtained and observations in dark field imaging using a two-beam condition. The existence of γ′ phase was also confirmed by an analysis of the SADPs. It is recognized that the size of γ″/γ′ particles in the 199 °C/min and 51 °C/min specimens is similar (Fig. 6a, b). The size of the in-grain precipitates was, on the other hand, 60 nm in the specimen with a slow cooling rate of 1 °C/min, which is 2–3 times as large as those observed in the specimens with the cooling rates of 199 and 51 °C/min.

Dependence of Microstructure on the Cooling Rate in the Solution Treatment

The observed dependence of microstructure on the cooling rate in the subsolvus solution treatment is summarized as follows:

(1) The size of γ″/γ′ precipitates in grains decreases with increasing the cooling rate from 1 to 51 °C/min but saturates above *these* cooling rate*s*.

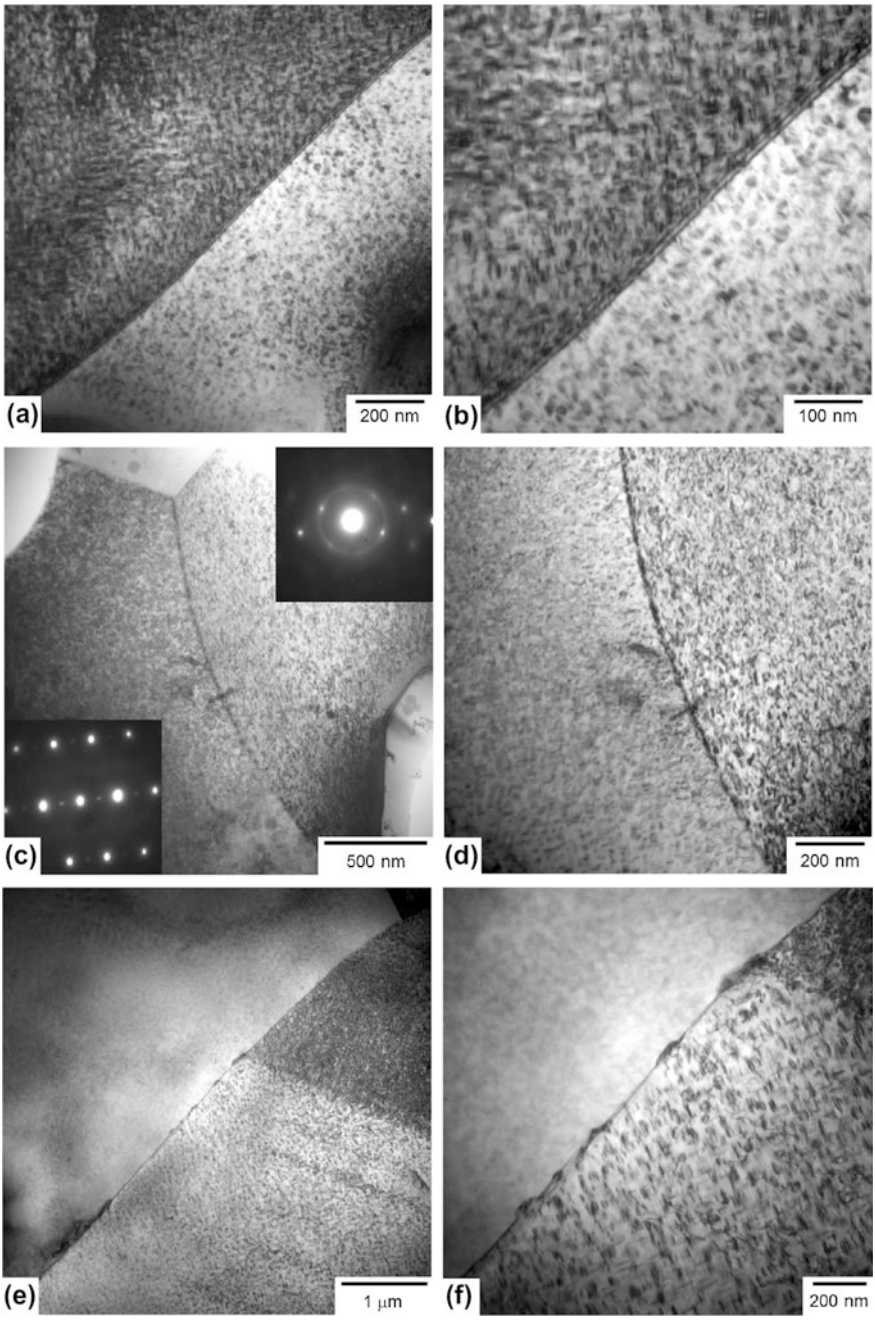

Fig. 5 Transmission electron images taken from areas including high angle grain boundaries in the gauge portion of the alloy 718 specimens after 0.2% creep strain: **a**, **b** 199 °C/min, **c**, **d** 51 °C/min, **e**, **f** 1 °C/min. Diffraction patterns in (**c**): B = 113 for the left grain, B ~ 110 for the right grain. The misorientation angle between the two grains is about 30°

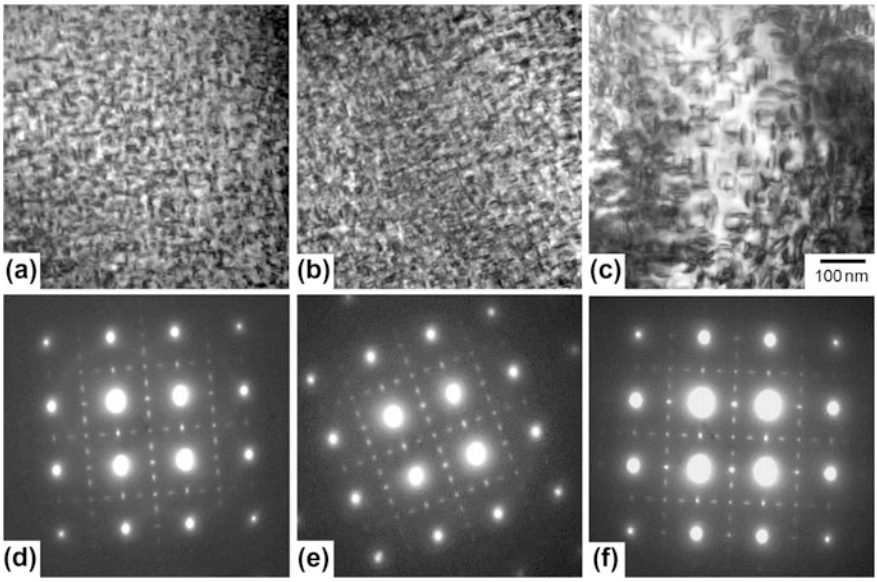

Fig. 6 Transmission electron images taken from grain interiors in the gauge portion of the alloy 718 specimens after 0.2% creep strain: **a–c** bright field images in the same magnification, **d–f** selected area diffraction patterns B = 001, **a**, **d** 199 °C/min, **b**, **e** 51 °C/min, **c**, **f** 1 °C/min

(2) *Precipitation* of γ″ phase is enhanced on grain boundaries and coherent twin boundaries at an intermediate cooling rate of 51 °C/min.
(3) δ phase platelets precipitate on grain boundaries and incoherent twin boundaries. This precipitation is pronounced as the cooling rate decreases.

The dependence of the precipitation of γ and δ phase on the cooling rate indicate that the precipitations occurred during cooling from the solution treatment. These results are not inconsistent with the results reported by Geng et al. [6].

The dependence of creep strength on the cooling rate is discussed below based on the microstructural features obtained in the present study. *It was confirmed that the lower creep strength at slower cooling rates is rationalized by coarser γ phase precipitate size and their smaller number density.* Chaturvedi et al. [7] prepared alloy 718 samples with different γ″ phase size in grains by changing the period of aging at 725 °C and found that the minimum creep rate of the samples shows a minimum at a γ″ phase size of 20–30 nm under a test condition at a temperature of 600 °C and various stress levels between 670 and 815 MPa. They explained this result by an effect of the γ″ size on the *ease* of dislocation glide and dislocation climb motions. This explanation is, however, not true for the faster cooling rates of the present case since the size of γ″ phase saturates at and above the cooling rates at

which the creep strength was maximized. Wisniewski and Beddoes [8] reported an improved creep strength by grain boundary serration in Waspaloy. A significant grain boundary serration was, however, not observed in the present case. The observed microstructural features and literature survey lead us to speculate that the reduced creep strength at higher cooling rates is related to a less enhanced precipitation of γ″ precipitates on grain/twin boundaries.

A positive effect of grain boundary precipitates on creep rupture strength has been reported so far under a low stress condition. Takeyama et al. [9] reported that the minimum creep rate decreased with increasing the area fraction of grain boundaries covered by W phase (A2) precipitates in a Ni-20Cr-20 W alloy, and called this strengthening effect 'grain boundary precipitation strengthening (GBPS)'. *Takeyama* [10] have recently found grain boundary precipitation inhibits local deformation around grain boundaries and thereby reducing the acceleration of creep rate, resulting in the extension of creep life. This GBPS effect has never been reported in high stress condition, as far as the authors know, and further investigations are therefore needed to conclude the effect of grain boundary precipitates on creep deformation under a high stress condition.

Summary

The present paper investigates the effect of cooling rate in the standard subsolvus solution treatment on microstructure in aged 718 alloy specimens after a creep deformation to 0.2% creep strain, and correlates with a maximized creep strength at an intermediate cooling rate. The main results are:

(1) The size of γ″/γ′ precipitates in grains decreases with increasing the cooling rate from 1 to 51 °C/min but saturates above the cooling rate.
(2) *Precipitation* of γ″ phase is enhanced on grain boundaries and coherent twin boundaries at an intermediate cooling rate of 51 °C/min.
(3) δ phase platelets precipitate on grain boundaries and incoherent twin boundaries. This precipitation is *more* pronounced as the cooling rate decreases.
(4) The dependence of creep strength on the cooling rate is explained such that the reduced creep strength at slower cooling rates is due to a coarser γ″ phase precipitate size and their smaller number density, and the reduced strength at higher cooling rates is related to a pronounced precipitation of γ″/γ′ precipitate particles on grain/twin boundaries.

References

1. Davis JR et al (eds) (2000) ASM specialty handbook: nickel, cobalt, and their alloys. ASM International, Materials Park OH, pp 33–36
2. Special Metals Homepage: www.specialmetals.com
3. Brown EE, Muzyka DR. In: Sims CT, Stoloff NS, Hagel WC (eds.) (1987) Superalloys II: high-temperature materials for aerospace and industrial power. A Wiley-Interscience Publication, Wiley, New York, p 165–188
4. Reed RC (2006) The superalloys: fundamentals and applications. Cambridge University Press, UK
5. Aoki C, Ueno T, Ohno T, (2015) Effects of solution heat treatment conditions on metallographic structures and mechanical properties of Alloy 718 (In Japanese). In: Proceedings of the 43rd annual meeting of gas turbine society of Japan A-11
6. Geng L, Na Y-S, Park N-K (1997) Continuous cooling transformation behavior of alloy 718. Mater Lett 30:401–405
7. Chaturvedi MC, Han Y (1989) Creep deformation of alloy 718. Superalloy 718:489–498
8. Wisniewski A, Beddoes J (2009) Influence of grain-boundary morphology on creep of a wrought Ni-base superalloy. Mater Sci Eng A 510–511:266–272
9. Takeyama M, Kawasaki K, Matsuo T, Tanaka R (1986) Effect of grain boundary precipitates on high temperature creep properties of Ni-20Cr-20 W alloys (In Japanese). Tetsu to Hagané 72:1605–1612
10. Takeyama M (2012) Recent trend on materials development for A-USC power plants (In Japanese). DENKI-SEIKO 83(1):27–33